ISSN: 2583-7346
DOI: https://doi-ds.org/doilink/05.2023-76281641/0005052023, May2023, Volume-1, Issue-2, pp. 1-10
International Journal of Advances in Engineering Architecture Science and Technology

Diagnostic Prototypical for Moment-Curvature Behaviour of Fibre Reinforced Concrete Beams

A. Arun Solomon[1*]

[1]Department of Civil Engineering, GMR Institute of Technology, Rajam, Andhra Pradesh, India

Received: 08-05-2023 **Accepted:** 26-05-2023 **Published:** 27-05-2023

Abstract

Background / Objectives: The association between the moment and curvature of reinforced sections is a very significant limit for the non-linear study of reinforced concrete construction. A strong opinion of the strength, stiffness, and energy dissipation capacity of the structure can be gotten from this association. The moment-curvature relationship would allow us to detect the strength decrease outside the topmost point and the degradation of the flexural inflexibility.
Methods / Statistical Analysis: Several methods have been utilised to study the response of concrete structural components.
Findings: To carry out the moment curvature analysis, a programme is written with and without steel fibres on plain and reinforced beams using MAT-LAB.
Applications / Improvements: The moment curvature analysis is a non-linear analysis done to find out the ductility factor, flexural strength, and flexural rigidity. Moment capacity increases simultaneously, and curvature also increases with varying steel fibres.

Key words: Moment-curvature, flexural rigidity, steel fibres, flexural strength

1. Introduction

The inherent weak tensile strength of concrete makes it prone to tensile cracking in tensile and flexural loadings and brings numerous problems to the application of this material, mainly in its durability. Reinforcement of cementitious materials with short, randomly distributed fibres has been successfully practised for more than 40 years. In fibre-reinforced cement (FRC) materials, reinforcing fibres allow crack bridging, a mechanism that improves the post-cracking residual strength of concrete by restraining crack opening. Debonding and pulling out of fibres dissipate energy, leading to a substantial increase in toughness, which enhances the energy absorption and ductility of the concrete composite.
The most fundamental requirement for predicting the moment curvature behaviour of a flexural member is knowledge of the behaviour of its constituents. With the increasing use of higher-grade concretes, whose ductility is significantly lower than normal concrete, it is essential to confine the concrete. In a flexure member, the shear reinforcement also confines the concrete in the compression zone. Hence, to predict the moment curvature behaviour of a flexural member, the stress–strain behaviour of confined concrete in axial compression is essential. With the development of performance-based design methods, there is an increasing need for simplified but reliable analytical tools capable of predicting the flexural behaviour of reinforced concrete members.

* A. Arun Solomon, Department of Civil Engineering, GMR Institute of Technology, Rajam, Andhra Pradesh, India. Email: arunsolomon.a@gmail.com

ISSN: 2583-7346
DOI: https://doi-ds.org/doilink/05.2023-76281641/0005052023, May2023, Volume-1, Issue-2, pp. 1-10
International Journal of Advances in Engineering Architecture Science and Technology

Tensile and compressive behavior of FRC material

Typical tensile stress-strain responses for plain and fibre-reinforced concrete are registered in experimental tensile tests. Curves obtained after different concrete ages are presented on the same diagram in order to show the behaviour as a function of the cement hydration development. For plain concrete, the stress-strain diagram demonstrates the brittle behaviour of the material. After peak stress, the residual strength decreases rapidly with increasing strain. When the macrocrack is localised, its propagation is very rapid and requires only low energy. In the fibre-reinforced concrete, however, the stress decay in the post-peak of the stress strain diagram is not as pronounced. In this case, due to the relatively large value of ultimate strain, the energy dissipation capacity is increased.

Benefits of fibres

- Distributes localised stresses.
- Reduction in maintenance and repair costs.
- Provides tough and durable surfaces.
- Reduces surface permeability, dusting, and wear.
- Cost saving.

2. Analytical Model for Fibre Reinforced Concrete

Tension and compression models for FRC

The moment curvature relationship of FRC material is generated by utilising the stress-strain (σ-ε) diagrams proposed by Soranakom and Mobasher, represented in Figure 1.

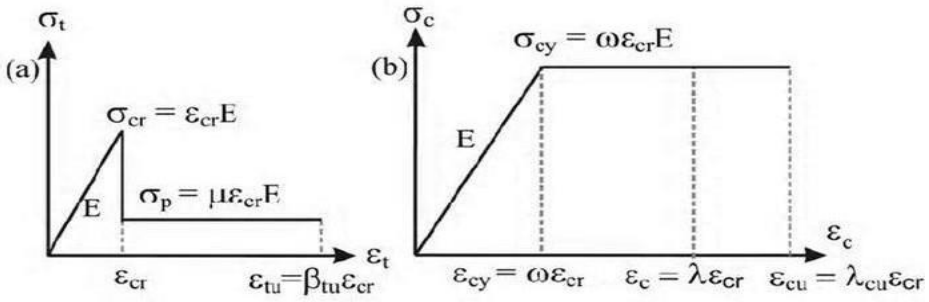

Figure 1. Fibre Reinforced Concrete Model (a) Tension Model (b) Compression Model

These diagrams are based on an idealised mode for steel fibre concrete. The first model represents a bilinear response for tension and compression, as shown in Figure 1. According to Figure 1 (a), the tension response increases linearly from the origin up to the cracking strain (εcr). After that, tensile stress remains constant at the post peak tensile strength (σp) which can be related to the ultimate tensile strength (σcr) by defining the normalised post-peak tensile strength (μ). This factor may be a function of the fibre volume fraction, geometry, stiffness, and bond characteristics of the fibres and also depend on the properties of the cement surrounding the fibres. The residual stress is assumed to be constant up to an ultimate strain (εcu).

ISSN: 2583-7346
DOI: https://doi-ds.org/doilink/05.2023-76281641/0005052023, May2023, Volume-1, Issue-2, pp. 1-10
International Journal of Advances in Engineering Architecture Science and Technology

Solutions for moment-curvature

The moment curvature diagram for a rectangular cross section of width *b* and depth *d* composed of FRC materials, can be derived in accordance with Figure 2. The distribution of tensile and compressive stresses in this figure 2 The three possible stages of tensile strain at the bottom fibre, $0 \leq \beta \leq 1$, $1 \leq \beta \leq \alpha$, and $\alpha \leq \beta \leq \beta tu$, are represented in Figures. 2a, 2b, and 2c, respectively. Each of Stages 2 and 3 has two possible conditions due to the value of compressive strain at the top fibre in either elastic ($0 \leq \lambda \leq \omega$) or plastic ($\omega \leq \lambda \leq \lambda cu$) behaviour in compression.

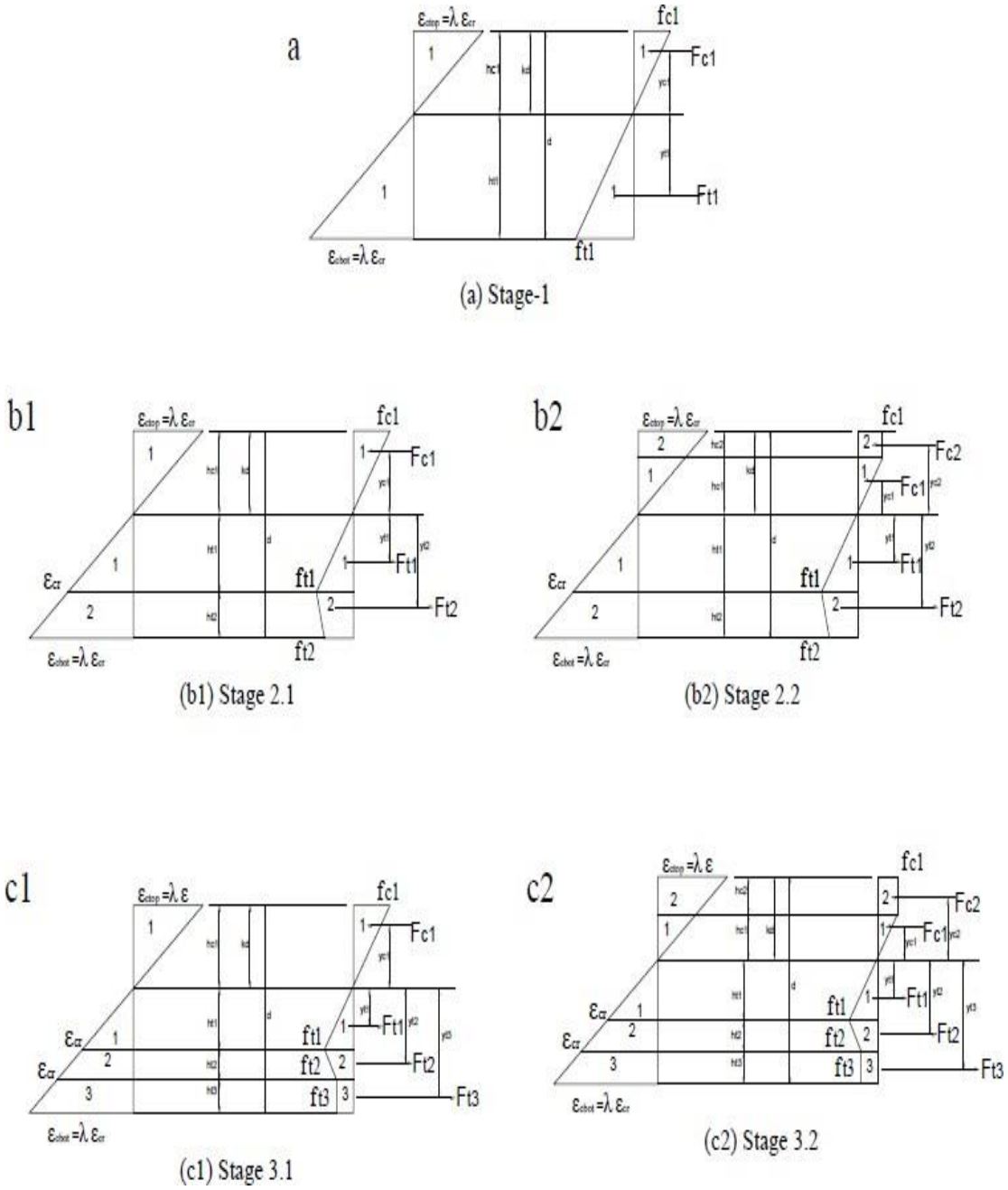

Figure 2. Stress-Strain Diagram at Different Stages of Normalized Tensile Strain at Bottom Fibre.

The deduction of the expressions in Tables 1 and 2 can be found elsewhere.

ISSN: 2583-7346
DOI: https://doi-ds.org/doilink/05.2023-76281641/0005052023, May2023, Volume-1, Issue-2, pp. 1-10
International Journal of Advances in Engineering Architecture Science and Technology

Table 1. Normalized Height of Compression and Tension Zones for Each Stage of Normalized Tensile Strain at Bottom Fibre (B)

Noralized height	Stage 1 $0 \le \beta \le 1$ $0 \le \lambda \le \omega$	Stage 2.1 $1 \le \beta \le \alpha$ $0 \le \lambda \le \omega$	Stage 2.2 $1 \le \beta \le \alpha$ $\omega < \lambda \le \lambda_{cu}$	Stage 3.1 $\beta > \alpha$ $0 \le \lambda \le \omega$	Stage 3.2 $\beta > \alpha$ $\omega < \lambda \le \lambda_{cu}$
h_{c2}/d	-	1	$(k\beta-\omega(1-k))/\beta$	-	$(k\beta-\omega(1-k))/\beta$
h_{c1}/d	K	K	$\omega(1-k)/\beta$	k	$\omega(1-k)/\beta$
h_{t1}/d	1-k	$(1-k)/\beta$	$(1-k)/\beta$	$(1-k)/\beta$	$(1-k)/\beta$
h_{t2}/d	-	$((1-k)(\beta-1))/\beta$	$((1-k)(\beta-1))/\beta$	$((1-k)(\alpha-1))/\beta$	$((1-k)(\alpha-1))/\beta$
h_{t3}/d	-	-	-	$((1-k)(\beta-\alpha))/\beta$	$((1-k)(\beta-\alpha))/\beta$

Table 2. Normalized Stress at Vertices in the Stress Diagram for Each Stage of Normalized Tensile Strain at Bottom Fibre (B)

Noralized stress	Stage 1 $0 \le \beta \le 1$ $0 \le \lambda \le \omega$	Stage 2.1 $1 \le \beta \le \alpha$ $0 \le \lambda \le \omega$	Stage 2.2 $1 \le \beta \le \alpha$ $\omega < \lambda \le \lambda_{cu}$	Stage 3.1 $\beta > \alpha$ $0 \le \lambda \le \omega$	Stage 3.2 $\beta > \alpha$ $\omega < \lambda \le \lambda_{cu}$
$f_{c2}/E\ \varepsilon_{cr}$	-	-	$\omega\Upsilon$	-	$\omega\Upsilon$
$f_{c1}/E\ \varepsilon_{cr}$	$\Upsilon\beta k/(1-k)$	$\Upsilon\beta k/(1-k)$	$\omega\Upsilon$	$\Upsilon\beta k/(1-k)$	$\omega\Upsilon$
$f_{t1}/E\ \varepsilon_{cr}$	B	1	1	1	1
$f_{t2}/E\ \varepsilon_{cr}$	-	$1+\eta\ (\beta-1)$	$1+\eta\ (\beta-1)$	$1+\eta\ (\alpha-1)$	$1+\eta\ (\alpha-1)$
$f_{t3}/E\ \varepsilon_{cr}$	-	-	-	μ	M

Table 3. Normalized Force Component for Each Stage of Normalized Tensile at Bottom Fibre(B)

Noralized stress	Stage 1 $0 \le \beta \le 1$ $0 \le \lambda \le \omega$		Stage 2.1 $1 \le \beta \le \alpha$ $0 \le \lambda \le \omega$	Stage 2.2 $1 \le \beta \le \alpha$ $\omega < \lambda \le \lambda_{cu}$	Stage 3.1 $\beta > \alpha$ $0 \le \lambda \le \omega$	Stage 3.2 $\beta > \alpha$ $\omega < \lambda \le \lambda_{cu}$
$F_{c2}/bdE\ \varepsilon_{cr}$	-		-	$\omega\Upsilon/\beta(\beta k+\omega k-\omega)$	-	$\omega\Upsilon/\beta(\beta k+\omega k-\omega)$
$F_{c1}/bdE\ \varepsilon_{cr}$	$(\beta\Upsilon k^{2})/2(1-k)$		$(\beta\Upsilon k^{2})/2(1-k)$	$(\omega^{2}\Upsilon/2\beta)(1-k)$	$(\beta\Upsilon k^{2})/2(1-k)$	$(\omega^{2}\Upsilon/2\beta)(1-k)$
$F_{t1}/bdE\ \varepsilon_{cr}$	$(\beta/2)(1-k)$		$(1-k)/2\beta$	$(1-k)/2\beta$	$(1-k)/2\beta$	$(1-k)/2\beta$
$F_{t2}/bdE\ \varepsilon_{cr}$	-		$((1-k)(\beta-1)(\eta\beta-\eta+2))/2\beta$	$((1-k)(\beta-1)(\eta\beta-\eta+2))/2\beta$	$((1-k)(\alpha-1)(\eta\alpha-\eta+2))/2\beta$	$((1-k)(\alpha-1)(\eta\alpha-\eta+2))/2\beta$
$F_{t3}/bdE\ \varepsilon_{cr}$	-		-	-	$((1-k)(\beta-\alpha)\mu)/\beta$	$((1-k)(\beta-\alpha)\mu)/\beta$

ISSN: 2583-7346
DOI: https://doi-ds.org/doilink/05.2023-76281641/0005052023, May2023, Volume-1, Issue-2, pp. 1-10
International Journal of Advances in Engineering Architecture Science and Technology

Table 4. Normalized Moment Arm of Force Component for Each Stage of Normalized Tensile Strain at Bottom Fibre (B)

Noralized stress	Stage 1 $0 \le \beta \le 1$ $0 \le \lambda \le \omega$	Stage 2.1 $1 \le \beta \le \alpha$ $0 \le \lambda \le \omega$	Stage 2.2 $1 \le \beta \le \alpha$ $\omega < \lambda \le \lambda_{cu}$	Stage 3.1 $\beta > \alpha$ $0 \le \lambda \le \omega$	Stage 3.2 $\beta > \alpha$ $\omega < \lambda \le \lambda_{cu}$
h_{c2}/d	-	1	$(k\beta-\omega(1-k))/\beta$	-	$(k\beta-\omega(1-k))/\beta$
h_{c1}/d	K	K	$\omega(1-k)/\beta$	k	$\omega(1-k)/\beta$
h_{t1}/d	1-k	$(1-k)/\beta$	$(1-k)/\beta$	$(1-k)/\beta$	$(1-k)/\beta$
h_{t2}/d	-	$((1-k)(\beta-1))/\beta$	$((1-k)(\beta-1))/\beta$	$((1-k)(\alpha-1))/\beta$	$((1-k)(\alpha-1))/\beta$
h_{t3}/d	-	-	-	$((1-k)(\beta-\alpha))/\beta$	$((1-k)(\beta-\alpha))/\beta$

Table 5. Equilibrium of Force, Moment and Curvature for Each Stage of Normalized Tensile Strain at Bottom Fibre (B)

Stage	K	M	ϕ
1	$k_{1=1/2}$ for $\Upsilon=1$ $k_{1=(-1+\sqrt{\Upsilon})/-1+\Upsilon}$ for $\Upsilon<1$ or $\Upsilon>1$	$M_1=(2\beta(\Upsilon-1)k_1^3+3k_1^2-3k_1+1])/1-k_1$	$\Phi_1=\beta/2(1-k_1)$
2.1	$K_{21}=(\beta 2\Upsilon+D_{21}-(\sqrt{\Upsilon^2\beta^4+D_{21}\Upsilon\beta^2}))/D_{21}$ $D_{21}=\eta(\beta^2-2\beta+1)+2\beta-\beta^2\Upsilon-1$	$M_{21}=((2\beta\Upsilon+C_{21})\,k_{21}^3-3C_{21}\,k_{21}^2+3C_{21}\,k_{21}-C_{21})/(1-k_2)$ $C_{21}=(-2\eta\beta^3+3\eta\beta^2-3\beta^2-\eta+1)/\beta^2$	$\Phi_{21}=\beta/2(1-k_{21})$
2.2	$K_{22}=D_{22}/D_{22}+2\omega\Upsilon\beta$ $D_{22}=\eta(\beta^2-2\beta+1)+2\beta+\omega^2\Upsilon-1$	$M_{21}=(3\omega\Upsilon+C_{22})\,k_{22}^2-2C_{22}\,k_{21}+C_{22}$ $C_{22}=(2\eta\beta^3-3\eta\beta^2+3\beta^2-\omega^3\Upsilon+\eta-1)/\beta^2$	$\Phi_{22}=\beta/2(1-k_{22})$
3.1	$K_{31}=(D_{31}-(\sqrt{\Upsilon\beta^2}\,D_{31}))/D_{31}-\beta^2\Upsilon$ $D_{31}=\eta(\alpha^2-2\alpha+1)+2\mu(\beta-\alpha)+2\alpha-1$	$M_{31}=((C_{31}-2\beta\Upsilon)\,k_{31}^3-3C_{31}\,k_{31}^2+3C_{31}\,k_{31}-C_{31})/(k_{31}-1)$ $C_{22}=(3(\mu\beta^2-\mu\alpha^2-\eta\alpha^2+\alpha^2)+2\eta\alpha^3+\eta-1)/\beta^2$	$\Phi_{31}=\beta/2(1-k_{31})$
3.2	$K_{32}=D_{32}/(D_{32}+2\omega\Upsilon\beta)$ $D_{32}=\omega^2\Upsilon+\eta\alpha^2+2(\mu\beta-\eta\alpha-\mu\alpha+\alpha)$	$M_{32}=(C_{32}+3\omega\Upsilon)K_{32}^2-2C_{32}K_{32}+C_{32}$ $C_{32}=(3(\mu\beta^2-\mu\alpha^2-\eta\alpha^2+\alpha^2)+2\eta\alpha^3-\omega^3\Upsilon+\eta-1)/\beta^2$	$\Phi_{32}=\beta/2(1-k_{32})$

Table 6. Neutral Axis Depth Ratio, Normalized Moment and Curvature for Each Stage of Normalized Tensile

Stage	Tension	Compression	Force equilibrium	Internal moment
1	$0 \le \beta \le 1$	$0 \le \lambda \le \omega$	$-F_{c1}+F_{t1}$	$F_{c1}\,y_{c1}+F_{t1}\,y_{t1}$
2.1	$1 < \beta \le \alpha$	$0 \le \lambda \le \omega$	$-F_{c1}+F_{t1}+F_{t2}$	$F_c\,y_{c11}+F_{t1}\,y_{t1}+F_{t2}\,y_{t2}$
2.2	$1 < \beta \le \alpha$	$\omega < \lambda \le \lambda_{cu}$	$-F_{c1}-F_{c2}+F_{t1}+F_{t2}$	$F_{c1}\,y_{c1}-F_{c2}\,y_{c2}+F_{t1}\,y_{t1}+F_{t2}\,y_{t2}$
3.1	$\beta > \alpha$	$0 \le \lambda \le \omega$	$-F_{c1}+F_{t1}+F_{t2}+F_{t3}$	$F_{c1}\,y_{c1}+F_{t1}\,y_{t1}+F_{t2}\,y_{t2}+F_{t3}\,y_{t3}$
3.2	$\beta > \alpha$	$\omega < \lambda \le \lambda_{cu}$	$-F_{c1}-F_{c2}+F_{t1}+F_{t2}+F_{t3}$	$F_{c1}y_{c1}-F_{c2}\,y_{c2}+F_{t1}\,y_{t1}+F_{t2}\,y_{t2}+F_{t3}\,y_{t3}$

ISSN: 2583-7346
DOI: https://doi-ds.org/doilink/05.2023-76281641/0005052023, May2023, Volume-1, Issue-2, pp. 1-10
International Journal of Advances in Engineering Architecture Science and Technology

3. Results and Discussions

Stress-Strain Response for SFRC Compression Test

After 28 days of curing, the cylindrical specimens were tested in a compression testing machine with a capacity of 200 tonnes. An extensometer with a gauge length of 200 mm and a least count of 0.002mm has been used to note the deformation values. The compressive strength of the specimen can be calculated by dividing the failure load by the cross-sectional area of the specimen.

Figure 2. Testing of Compressive Strength Test Specimen

Tensile Test

Figure 3. Test Set Up of Specimen Under UTM

The development of moment-curvature relations for rectangular RC beam sections and the effect of different parameters (such as steel fibre reinforced concrete and reinforced concrete with varying percentages of fibre volume in M30 grade concrete such as 0%, 0.5%, 1%, and 1.5%)

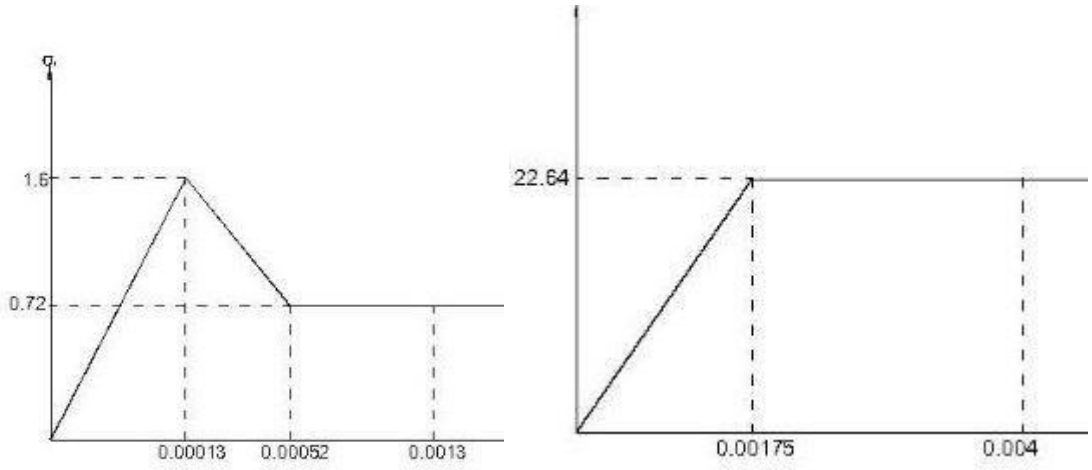

Figure 4. Tension And Compressive Response of FRC with 0% Fibre

ISSN: 2583-7346
DOI: https://doi-ds.org/doilink/05.2023-76281641/0005052023, May2023, Volume-1, Issue-2, pp. 1-10
International Journal of Advances in Engineering Architecture Science and Technology

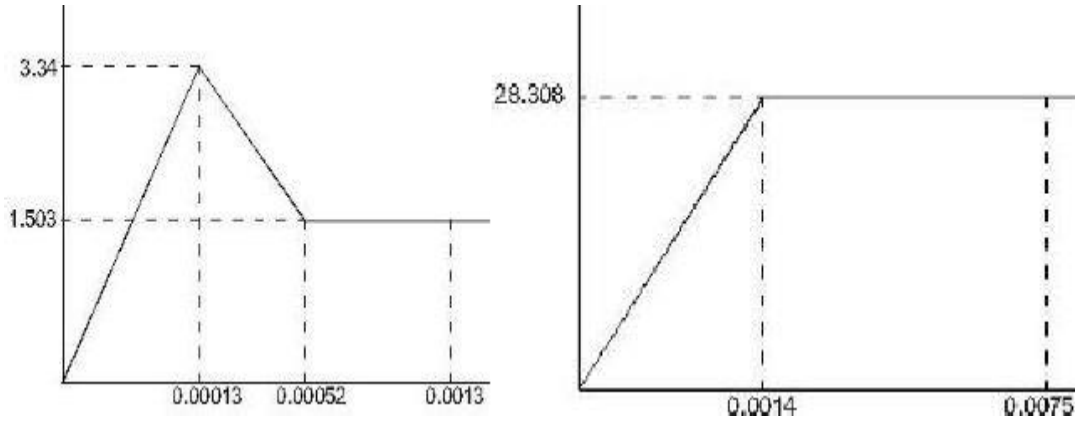

Figure 5. Tension and Compressive Response of FRC with 0.5% Fibre

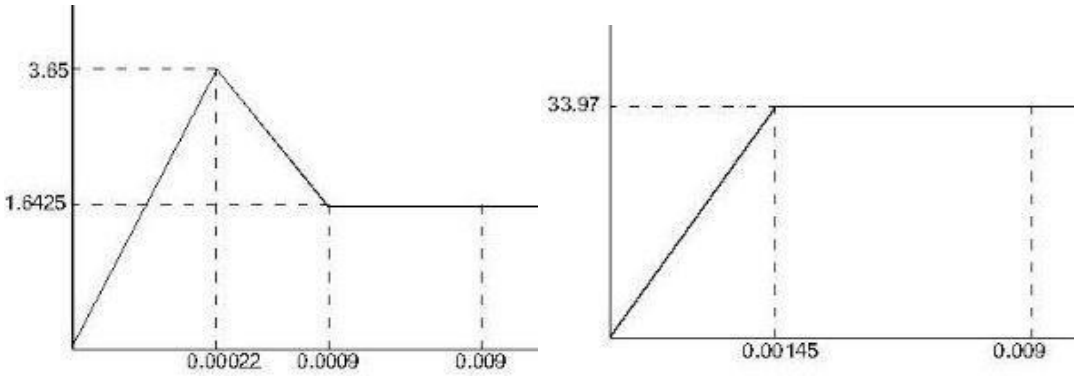

Figure 6. Tension and Compressive Response of FRC with 1% Fibre

Table 7. Tension and Compressive Response of FRC with 1.5% Fibre

	Tension					Compression		
% of fibre	**ε_{cr}**	**ε_{trn}**	**ε_{tu}**	**σ_{cr} (MPa)**	**σ_{cst} (MPa)**	**ε_{cy}**	**ε_{cu}**	**σ_{cy} (MPa)**
0 %	0.00013	0.00052	0.0013	1.6	0.72	0.00175	0.004	22.64
0.5 %	0.00013	0.00052	0.0013	3.34	1.503	0.0014	0.0075	28.31
1 %	0.0002	0.0009	0.009	3.65	1.64	0.00145	0.009	33.97
1.5 %	0.00026	0.001	0.0026	2.93	1.319	0.00074	0.0048	22.64

Moment-Curvature Relationship of SFRC

A moment-curvature diagram for a particular crossection is plotted with the x-axis representing the curvature and the y-axis representing the moment. A typical example of the moment-curvature relationship of the material is as follows:

1. The curve is linear until material yield; the moment is directly proportional to curvature. The slope of the curve represents the flexural rigidity of the section within its elastic limit.
2. The curve is nonlinear after material yield. This stage represents the hardening behaviour of the section against the moment as well as the ductility of the section.

ISSN: 2583-7346
DOI: https://doi-ds.org/doilink/05.2023-76281641/0005052023, May2023, Volume-1, Issue-2, pp. 1-10
International Journal of Advances in Engineering Architecture Science and Technology

3. The curve falls down after the peak moment, this stage represents the softening behaviour of the section.
4. This stage represents the debonding of composites present in the member, as the critical crack forms, the member/section will fail suddenly.

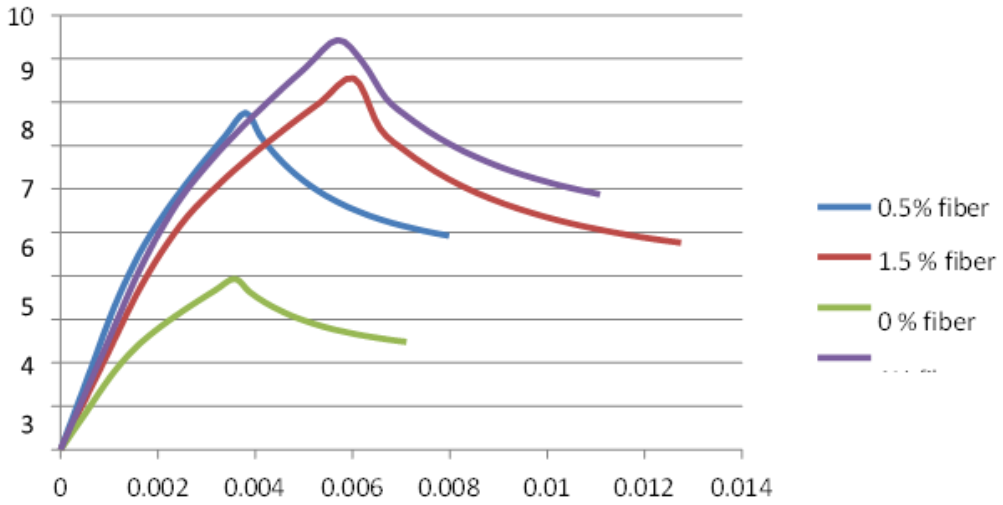

Figure 7. Moment Curvature Relationship for 0%, 0.5%, 1% and 1.5% Fibre

5. The improvement in flexural rigidity is 6%, 33.46%, and 65% due to the addition of steel fibres in 0.5%, 1%, and 1.5% by volume of concrete, respectively, compared with 0% fibre fraction.
6. The improvement in ductility factor is 11.17%, 13%, and 17% due to the addition of steel fibres in 0.5%, 1%, and 1.5% by volume of concrete, respectively, compared with 0% fibre fraction.
7. The improvement in flexural strength is 96.97%, 139.56%, and 117.1% due to the addition of steel fibres in 0.5%, 1%, and 1.5% by volume of concrete, respectively, compared with 0% fibre fraction.

4. Test Results

Table 8. Test Result

	Fibres (%)	**Flexural rigidity (KN-m^2)**	**Percentage of increment**	**Ductility factor**	**% of increment**	**Flexural strength (KN/m^2)**	**% of increment**
% of steel fibres of M30 grade	0	1242.9	0%	3.08	0%	3782.4	0%
	0.5	1418.57	6%	3.424	11.17 %	7450.56	96.97%
	1	1658.87	33.46 %	3.510	13%	9061.44	139.56%
	1.5	2053.17	65%	3.606	17%	8211.84	117.1%

ISSN: 2583-7346
DOI: https://doi-ds.org/doilink/05.2023-76281641/0005052023, May2023, Volume-1, Issue-2, pp. 1-10
International Journal of Advances in Engineering Architecture Science and Technology

5. Conclusions

The moment-curvature behaviour of normal steel reinforced fibre concrete beams was investigated in this research. The beams have 100×250×1250 mm dimensions. The moment Curvature behaviours were obtained and evaluated with the addition of fibres (from 0 to 1.5%). And also evaluated in terms of ductility factor, flexural strength, and flexural rigidity.

- The addition of steel fibres to the concrete improved the moment and
- The improvement of ultimate moment and curvature is 48% to 96.97% and 19.24 % to 90.22%, respectively, due to the addition of steel fibres in a 0.5% to 1.50% volume of
- The improvement in flexural rigidity is 6%, 33.46%, and 65% due to the addition of steel fibres in 5%, 1%, and 1.5% by volume of concrete, respectively, compared with 0% fibre fraction.
- The improvement in ductility factor is 11.17%, 13%, and 17% due to the addition of steel fibres in 0.5%, 1%, and 1.5% by volume of concrete, respectively, compared with 0% fibre fraction.
- The improvement in flexural strength is 96.97%, 139.56%, and 117.1% due to the addition of steel fibres in 0.5%, 1%, and 1.5% by volume of concrete, respectively, compared with 0% fibre fraction.

References

1. Kang, S.T., Lee, Y., Park, Y.D., and Kim, J.K., (2010), “Tensile fracture properties of an Ultra High Performance Fiber Reinforced Concrete (UHPFRC) with steel fiber”, Composite Structures, 92, p. 61-71.
2. ACI 440.2R-08. Guide for the design and construction of externally bonded FRP systems for strengthening concrete structures, Reported by American Concrete Institute, 80 p, July 2008.
3. Camps, G., Turatsinze, A., Sellier, A., Escadeillas, G., and Bourbon, X., (2008), “Steel-fiber reinforcement and hydration coupled effects on concrete tensile behavior”, Engineering Fracture Mechanics, 75, p. 5207-5216.
4. V.M.C.F. Cunha, J.A.O. Barros, J.M. Sena-Cruz. “Pullout behavior of steel fibers in self compacting concrete”, ASCE Journal of Materials in Civil Engineering, 22(1), January 2010.
5. Soranakom, C., Mobasher, B., (2009), “Flexural design of fiber-reinforced concrete”, ACI Materials Journals, p. 461-469.
6. Soranakom, C., Mobasher, B., (2008), “Correlation of tensile and flexural response of strain softening and strain hardening cement composites”, Cement & Concrete Composites, 30, p. 465- 477.
7. Soranakom, C., Mobasher, B., (2007), “Closed form solutions for flexural response o fiber reinforced concrete beams”, ASCE Journal of Engineering Mechanics Division (In Press).
8. Lim, T.Y., Paramasivam, P., and Lee, S.L. (1987), “Analytical model for tensile behavior of steel-fiber concrete”, ACI Material Journal, 84(4), p. 286-551.
9. Taheri, M.; Salehian, H.R., Barros, J.A.O., “A design model for strain-softening and strain hardening fiber reinforced elements failing in bending – implementation and

parametric studies", Technical report 24-DEC/E-09, Dep. Civil Eng., School Eng. University of Minho, December 2009.

10. Ersoy, U., Özcebe, G., (1998), "Moment-curvature relationship of confined concrete sections", Middle East Technical University, Department of Civil Engineering, Ankara, Teknik Dergi, 9(4), p. 1799-1827.
11. Basto, C.A.A.; Barros, J.A.O., "Numeric simulation of sections submitted to bending", Technical report 08-DEC/E-46, Dep. Civil Eng., School Eng. University of Minho, pp. 73, August 2008.
12. Eurocode 2: Design of concrete structures - Part 1: General rules and rules for buildings, April 2002.
13. Rossi, P., "High-Performance Multimodal Fiber-Reinforced Cement Composites (HPM-FRCC): the LCPC Experience," ACI Materials Journal, V. 94, No. 6, Nov.-Dec. 1997, pp. 478-483.
14. Danzer, R., "A General Strength Distribution Function for Brittle Materials," Journal of the European Ceramic Society, V. 10, No. 6, 1992, pp. 461-472.
15. Wee, T. H.; Lu, H. R.; and Swaddiwudhipong, S., "Tensile Strain Capacity of Concrete under Various States of Stress," Magazine of Concrete Research, V. 52, No. 3, June 2000, pp. 185-193.
16. Lankard, D. R., and Lease, D. H., "Highly Reinforced Precast Monolithic Refractories," American Ceramic Society Bulletin, V. 61, No. 7, July 1982, pp. 728-732.